www.sciencemag.org/content/345/6204/1616/suppl/DC1

Supplementary Material for

A critical time window for dopamine actions on the structural plasticity of dendritic spines

Sho Yagishita, Akiko Hayashi-Takagi, Graham C.R. Ellis-Davies, Hidetoshi Urakubo, Shin Ishii, Haruo Kasai*

*Corresponding author. E-mail: hkasai@m.u-tokyo.ac.jp

Published 26 September 2014, *Science* **345**, 1616 (2014)
DOI: 10.1126/science.1255514

This PDF file includes:

Materials and Methods

Adeno-associated virus (AAV) preparation and animal surgery

We prepared PPTA-mCherry AAV vectors to label the D1R-MSNs that constitute the direct pathway. For the construction of pAAV-PPTA-mCherry and pAAV-PPTA-Cre, the PPTA promoter was cloned from the mouse as described previously (*31*) and fused to mCherry or Cre and cloned into a AAV-expression vector derived from pAAV-EF1-DIO-hChR2(H134R)-mCherry, a kind gift from K. Deisseroth. AAV vectors were prepared and titred as described previously (*32*). Briefly, plasmids for AAV vector, pHelper (Stratagene), and RepCap5 (Applied Viromics) were transfected to HEK293 cells (AAV293, Stratagene). After a 3-d incubation, cells were collected and purified by CsCl-gradient ultracentrifugation. CsCl was removed by dialysis. Titres for AAV were estimated by quantitative polymerase chain reaction (qPCR). An AAV vector for EF1-DIO-hChR2(H134R) was purchased from the U Penn Vector core. A total of 1 µl AAV was injected bilaterally into nucleus accumbens (NAc; AP +1.3 mm, ML +/− 1.1 mm, DV + 4.3 mm) and ventral tegmental area (VTA; AP −3.4 mm, ML +/− 0.5 mm, DV +4.3 mm) of 3-week old DAT-IRES-Cre mice (B6.SJL-Slc6a3$^{tm1.1(cre)Bkmn}$/J, The Jackson Laboratory) with the infusion syringe pump (0.5 µl/min). Mice were allowed to recover for more than 2 weeks after the injection.

Acute slice preparation

Acute coronal slices of nucleus accumbens (280 µm) were obtained from 5- to 7-week-old mice that were injected with AAV. Mice were anesthetized by ketamine and xylazine; perfused transcardially by ice-cold solution containing 220 mM sucrose, 3 mM KCl, 8 mM $MgCl_2$, 1.25 mM NaH_2PO_4, 26 mM $NaHCO_3$, and 25 mM glucose; and then quickly decapitated to prepare slices with a VT1200 microtome (Leica). The slices were incubated at 34°C for 30 min and then at room temperature in artificial cerebrospinal fluid (ACSF; 125 mM NaCl, 2.5 mM KCl, 1 mM $CaCl_2$, 2 mM $MgCl_2$, 1.25 mM NaH_2PO_4, 26 mM $NaHCO_3$, and 20 mM glucose), which was bubbled with 95% O_2 and 5% CO_2. The slices were transferred to a recording chamber and superfused with the same ACSF above except for 2 mM $CaCl_2$, 1 mM $MgCl_2$, and 200 µM Trolox (Sigma). All physiological experiments were performed at 30–32°C.

In experiments with D-AP5 (50 µM, Tocris), KN62 (3 µM, Wako), SCH23390 (3 µM, Wako), sulpiride (10 µM, Wako), KT5720 (2 µM, Sigma-Aldrich), calyculin A (50 nM, Wako), tautomycetin (4 nM, Tocris), and papaverine (*25*) (10 µM, Wako), slices were superfused for at least 30 min with each inhibitor before glutamate uncaging. In experiments with anisomycin (5 µM, Sigma-Aldrich), slices were incubated with anisomycin for at least 1 h before glutamate uncaging. The experimental protocol was approved by the Animal Experimental Committee of the Faculty of Medicine, the University of Tokyo.

Two-photon imaging

Two-photon imaging of dendritic spines was performed with an upright microscope (BX61WI, Olympus) equipped with an FV1000 laser-scanning microscope

system (FV1000, Olympus) and a water-immersion objective lens (LUMPlanFI/IR, 60×, numerical aperture 1.0). The system included two mode-locked, femtosecond-pulse Ti:sapphire lasers (MaiTai from Spectra Physics). One was set at a wavelength of 720 nm for the uncaging of glutamate and the other was set at 980 nm for Alexa 488 and Fluo-4FF or 940 nm for Förster resonance energy transfer (FRET) imaging. Each of the lasers was connected to the microscope via an independent scan head and gated with an acoustico-optic modulator for two-photon uncaging of caged-glutamate and imaging. For ChR2 stimulation, optical fibre (500 μm core, BFH22-550, Thorlab) connected to a blue diode laser (457 nm, 15−20 mW, 5 ms, Lucir) was placed near the imaging site (~300 μm).

Dendrites containing spines within 100 μm from the soma (typically the second to fourth branches) and 20−35 μm in depth were used for the imaging and uncaging experiments unless otherwise noted. Three-dimensional reconstructions of dendritic morphology were generated by the summation of fluorescent values separated by 0.5 μm. The fluorescence of dendrites continued to increase gradually even 20 min after whole-cell perfusion and was corrected by the entire fluorescence of an imaging area where dendritic fluorescent signals were predominant. The spine-head volumes were estimated from the total fluorescence intensity. Neighboring spines were defined as spines within 3 μm of the stimulated spines.

Electrophysiology

For whole-cell recordings, the patch-clamp electrode (open-tip resistance, 5−8 MΩ) was filled with a solution containing 120 mM potassium gluconate, 20 mM KCl, 10 mM disodium phosphocreatine, 50 μM Alexa 488 (Life Technologies), 4 mM ATP (magnesium salt), 0.3 mM GTP (sodium salt), 10 mM HEPES, and 5 μM β-actin (human platelets; Cytoskeleton). The pH was adjusted to 7.25 with KOH, and the osmolarity was adjusted to 275−280 mOsm/l with sucrose. In experiments with protein kinase A inhibitor (PKI , 10 μM PKI [5−24] , Promega), autocamtide-2-related inhibitory peptide (AIP; 5 μM, Sigma-Aldrich), NB001 (50 μM, Sigma-Aldrich)(*33*, *34*), dopamine- and cAMP-regulated phosphoprotein 32 kDa (DARPP-32) inhibitory peptide (*18*) (DARPP-32 [1−22], 100 μM, BEX, custom peptide synthesis), DARPP-32 control peptide (DARPP-32 [8−22], 100 μM, BEX, custom peptide synthesis), inhibitors were included in the recording pipette and were allowed to perfuse at least 20 min after beginning whole-cell recording. The cells were voltage-clamped at −70 mV except during stimulation. Cells with a resting potential >−60 mV during the stimulating period were discarded before plasticity induction.

CDNI-glutamate (*35*) (4 mM) was locally pressure-puffed from a glass pipette positioned close to the selected dendrite. For experiments with continuous application of dopamine, dopamine (100 μM) (*36*) was also included in the puff pipette. The laser power was set 5−6 mW with activation time of 0.6 ms to evoke currents through AMPA (α-amino-3-hydroxy-5-methyl-4-isoxazolepropionic acid)-sensitive glutamate receptors with an amplitude of approximately 5–20 pA. This stimulation also evoked excitatory-postsynaptic potentials (EPSPs) similar to miniature excitatory-postsynaptic potentials (mEPSPs, fig. S1D). The signals were evoked three to five times at each time point, low-

pass filtered at 2 kHz, sampled at 10 kHz, and then averaged. For each experiment, ChR2 expression at the presynaptic fibers was confirmed by evoking an excitatory postsynaptic current (EPSC) with blue laser stimulation, which co-releases glutamate from the DA fiber (*37*).

Structural plasticity was induced by the following spike-timing-dependent plasticity (STDP) protocol (*15*) consisted of 15 trains of 10 bursts repeated at 0.1 Hz. Each burst was composed of three back-propagating APs (bAPs, 100 Hz) preceded by a single 2pEPSP ($\Delta t = +10$ ms) stimulated by two-photon uncaging of CDNI-glutamate at a wavelength of 720 nm. For each experiment, three to four spines were stimulated. To mimic the up-state, which may facilitate plasticity induction, a small depolarizing holding current (~120 pA) was applied to maintain voltage near −55 mV from 100 ms before the onset until the end of STDP stimulation (in total, 1.1 s). APs were induced by injection of a depolarizing current of 0.6−1 nA for 2 ms. The STDP protocol was combined with optical stimulation (457 nm, 5 ms, 30 Hz, 10 times) of dopaminergic fibers expressing ChR2 (DA_{opto}) at various time points relative to the onset of STDP stimulation.

To examine long-term potentiation of EPSCs (fig. S4), the same STDP protocol was used, except that glutamate uncaging was replaced with electrical stimulation of presynaptic fibers with theta-glass electrode (2 ms, 12−50 μA) which was placed 80−150 μm from the patch pipette. Test stimuli were applied every 15 s. Data were excluded when the series resistance changed more than 20 % over the time course of the experiment.

Amperometry

We confirmed that the optogenetically induced signal occurred at the peak current at 0.6 mV, which is consistent with the dopamine-induced oxidation current, using fast-scan cyclic voltammetry (from −0.5 V to 1.2 V at rate of 400V/s, scanning rate 10 Hz). The temporal characteristic of dopamine release in response to optogenetic stimulation was evaluated by constant-potential amperometry (*38*), which has high temporal resolution. Carbon-fibre microelectrodes with a small tip (Carbostar-1, 5−8 μm diameter, ~20 μm length, Kation Scientific) were placed 40−60 μm below the surface of the nucleus accumbens slice. The electrode potential was held at a constant voltage of 600 mV versus Ag/AgCl by ChemClamp (Dagan). Electrodes were calibrated with 0, 1, and 5 μM dopamine hydrochloride (Wako) in ACSF.

Ca^{2+} imaging

For Ca^{2+} measurements, the pipette solution contained Ca^{2+} sensitive 500 μM Fluo-4FF (Life Technologies) and non-sensitive 50 μM Alexa 594 (Life Technologies) fluorescent dye instead of Alexa 488. Images were acquired at 10 Hz. Fluorescence intensities were measured at 485−555 nm (G) and 598−672 nm (R) for Fluo-4FF and Alexa 594, respectively. We obtained the ratios $\Delta G/G_0 = (G(t)-G_0)/G_0$, where $G(t)$ is the fluorescence intensity at time t, and G_0 is the average intensity before stimulation.

Förster resonance energy transfer (FRET) imaging

AAV expression vectors carrying FRET probes were constructed by replacing CaMKII(0.3) promoter with EF1 and hChR2(H134R)-mCherry with Camuiα-CR or AKAR2-CR (*22*), which were kind gift from Dr. Lin. For CaMKII FRET imaging, D1R-MSNs were sparsely labelled (39) by co-injection of diluted PPTA-Cre and high titre CaMKII(0.3)-DIO-Camuiα-CR AAV vectors to nucleus accumbens. An AAV vector for EF1-DIO-hChR2(H134R)-mCherry was also injected into the ventral tegmental area. For PKA FRET imaging, an AAV vector expressing AKAR2-CR was injected instead of Camuiα-CR. Images were acquired at 2 Hz for distal dendrite and spine imaging with a single stack and 0.5 Hz with three to five stacks for soma and adjacent dendrite imaging. Fluorescence intensities were measured at 485−555 nm (*G*) and 598−672 nm (*R*) for Clover and mRuby2, respectively. Images were down sampled to 0.16 Hz for distal dendrites or 0.08 Hz for soma to improve the signal-to-noise ratio, and XY image drift was registered to the first image. For each region-of-interest (spine, dendrite, or soma), we obtained the ratios $\Delta r/r_0 = (r(t)-r_0)/r_0$, where $r(t)$ is the ratio of fluorescence intensity in G and R at time t, and r_0 is the average ratio before stimulation. Specifically, the $r(t)$ for Camuiα-CR activation was calculated as G divided by R, and $r(t)$ for AKAR2-CR activation was calculated as R divided by G, so that $\Delta r/r_0$ indicates the increase in the activity of each kinase that the FRET probe monitors. Channel bleeding was not corrected. For image display, Gaussian convolution with a standard deviation (SD) of 10 pixels, which corresponded to 0.55 μm for images of distal dendrites and 1.1 μm for images of soma, was applied for each G and R. The ratio images were created by calculating the ratio for each pixel, and then, the images were normalized to the images before stimulation and the relative ratio increases were pseudocolor coded.

Immunohistochemistry

The specificity of gene expression by AAV was assessed by immunohistochemistry. Mice injected with AAV were allowed to incubate more than 2 weeks and then were anesthetized (ketamine, xylazine) and perfused transcardially with 4% paraformaldehyde in phosphate-buffered saline (PBS). Slices (60-μm thick) containing the nucleus accumbens or ventral tegmental area were prepared using a vibratome. For nucleus accumbens slices, antigen retrieval was made by 10 mM sodium citrate for 30 min at 80°C. The slices were incubated with either anti-substance P (SA1270, Enzo Life Sciences, 1:400), anti-Met-enkephalin (EA1150, Enzo Life Sciences, 1:400) or anti tyrosine hydroxylase antibody (AB152, Millipore, 1:400−800) in PBS containing 5% normal goat serum, 0.2% Triton X, and 0.1% NaN_3 for 48 h at 4°C. After washing with PBS, slices were incubated with Anti-rabbit IgG antibody conjugated with Alexa488 (1:400) for 2 h at room temperature, then reacted with TO-PRO-3 (Life Technologies) for nuclear staining. The slices were mounted with anti-fading reagents (Vectashield, Vector Laboratories) and Z-stack images were acquired with confocal microscopy (BX-61, Olympus). The images were analyzed using ImageJ. For each of neuron expressing mCherry either driven by the PPTA promoter or fused with ChR2, the immunofluorescent signal was regarded as positive for the cell if the Alexa 488 signal continuously covered more than half of the soma at the Z level of peak TO-PRO-3 fluorescence.

Data analysis

Two-photon images were analyzed with ImageJ (National Institutes of Health) and a custom-made program running on Matlab (Mathworks Inc.). The electrophysiological data analyses and all statistical analyses were performed with Excel (Microsoft) and Excel Statistics (SSRI). For all spine volume analyses, volume changes at 40 min and 50 min after plasticity induction were averaged and used in the statistical analyses. For calcium imaging, the peak values (1 s after stimulation onset) were used in the statistical analyses. For FRET imaging, the averaged values of the time points spanning 12 s around the peak were included in the statistical analyses. Data are presented as mean ± s.e.m., and differences were analyzed by Mann-Whitney U tests or Kruskal–Wallis one-way analysis of variance (ANOVA) followed by Steel's post hoc test. $P < 0.05$ was considered statistically significant.

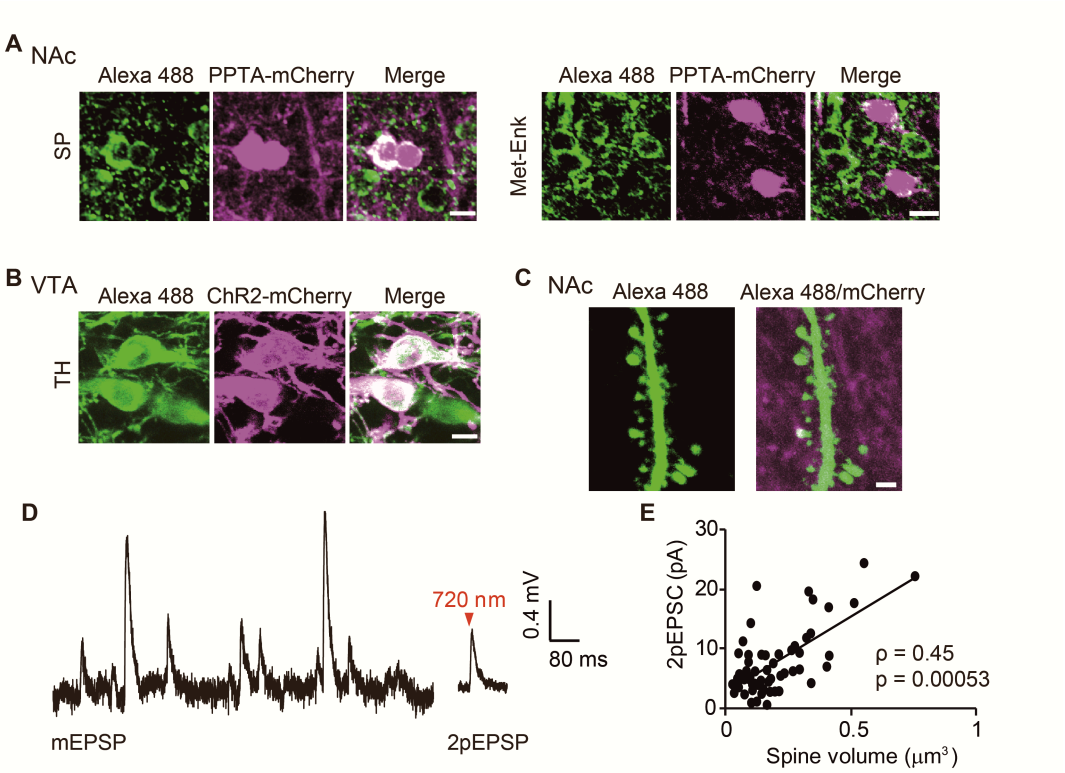

Fig. S1. Immunohistochemistry and two-photon glutamate uncaging.

(**A**) Immunohistochemical analysis of NAc slices expressing mCherry under the control of a PPTA promoter with anti-substance-P (left) or anti-met-enkephalin antibody labeled by secondary antibody conjugated with Alexa 488 (right). The fluorescence signal of mCherry overlapped with the D1R-MSN marker substance P but not with the D2R-MSN marker met-enkephalin (*14*). Among 95 neurons expressing mCherry, 85 (89%) neurons were positive for substance-P. In contrast, among 76 neurons expressing mCherry, 11 (14%) neurons were positive for met-enkephalin. SP, anti-substance P antibody, Met-Enk, anti-met-enkephalin antibody. Scale bar, 10 μm. (**B**) Immunohistochemical analysis of VTA slices expressing mCherry fused with hChR2 with anti-tyrosine hydroxylase antibody with Alexa 488. Among 195 neurons expressing mCherry, 184 (94%) neurons were positive for tyrosine hydroxylase. Scale bar, 10 μm. (**C**) Visualization of dendritic spines from a D1R-MSN with fluorescence emitted by Alexa 488 loaded through the recording pipette, and the overlay image on the ChR2-mCherry-expressing dopaminergic fibers and PPTA-mCherry-expressing neurites of MSNs. Scale bar, 2 μm. (**D**) Current clamp recording from an identified D1R-MSN showing an mEPSP (left) and two-photon uncaging of caged glutamate-induced EPSP (2pEPSP). The 2pEPSP is the average of five recordings. (**E**) Spine structure-functional relationship in MSNs (56 spines). Spine volumes and the peak 2pEPSC amplitudes for individual spines were plotted. The Spearman's correlation coefficient was 0.45 with $P = 0.00053$.

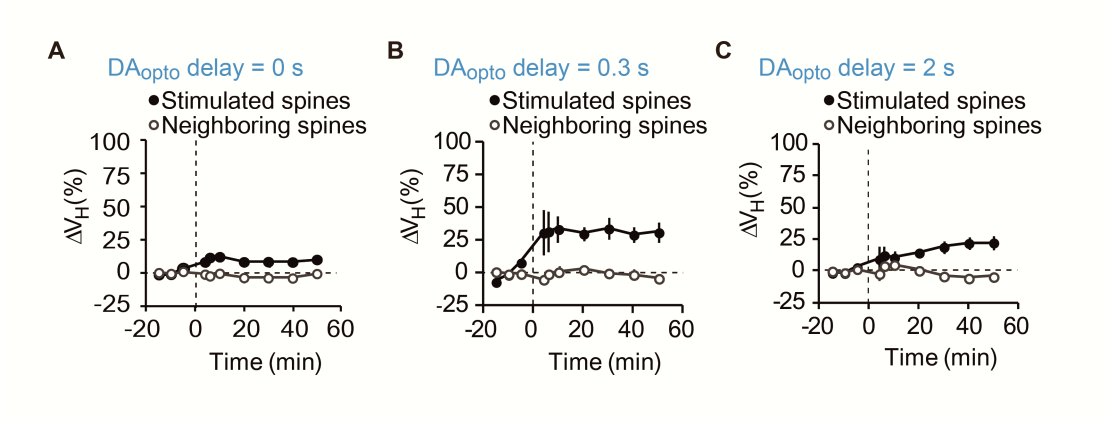

Fig. S2. Various DA_{opto} delays in STDP spine enlargement.

(**A–C**) Time courses of spine volume changes following STDP + DA_{opto} with delays of 0 s (A, 42 spines, 10 dendrites), 0.3 s (B, 20 spines, 5 dendrites), and 2 s (C, 28 spines, 7 dendrites). Data are presented as mean ± s.e.m for stimulated and neighboring spines.

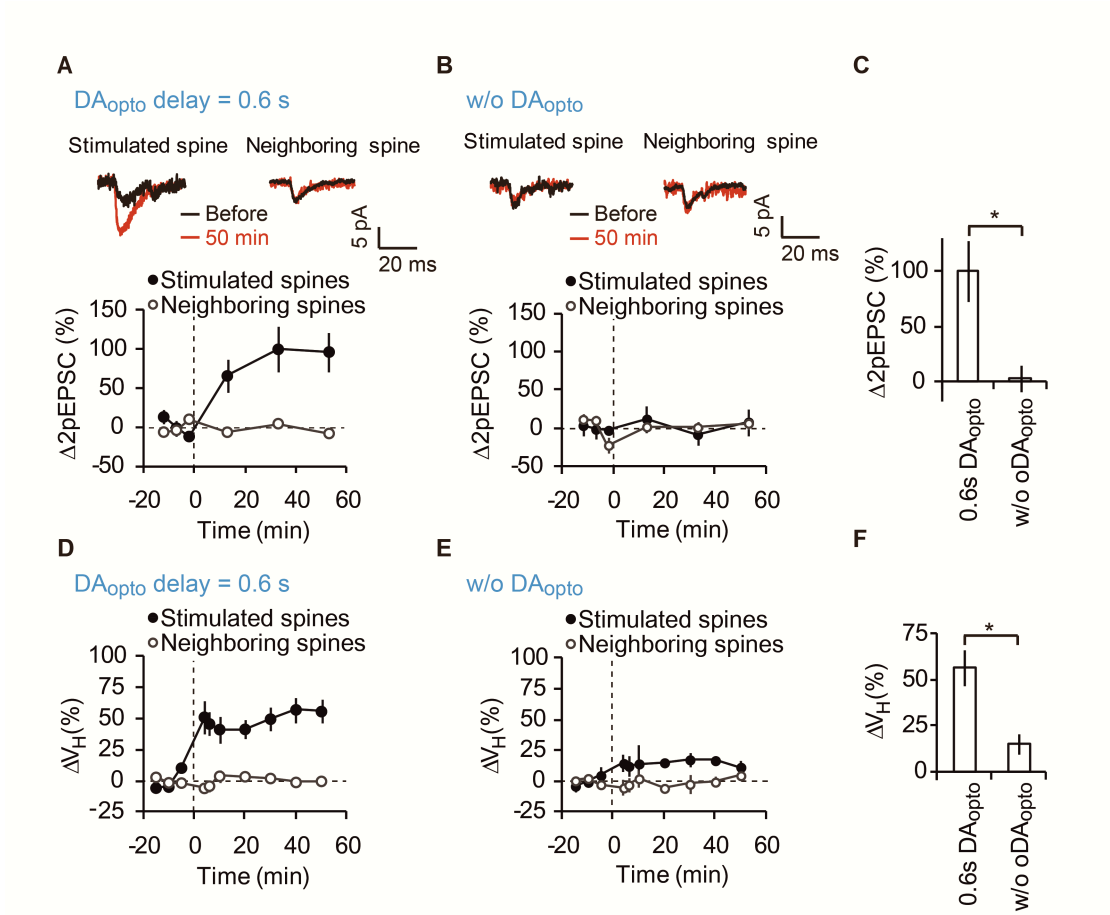

Fig. S3. Increases in 2pEPSCs accompanied spine enlargement.

(**A, B, D, E**) Time courses of the 2pEPSC amplitudes (A, 10 spines, 6 dendrites; B, 7 spines, 4 dendrites) and spine volume (D, E) in response to STDP + DA_{opto} with delays of 0.6 s (A, D) or without DA_{opto} (B, E). The data for 2pEPSC and spine volume were derived from the same spines. Insets in (A, B) show 2pEPSC for stimulated and neighboring spines before (black) and after the STDP protocol (red). (**C**, **F**), Average changes in 2pEPSCs (C) and spine volumes (F). Data are presented as mean ± s.e.m. * P = 0.033 (C) and 0.033 (F) with Mann-Whitney U test.

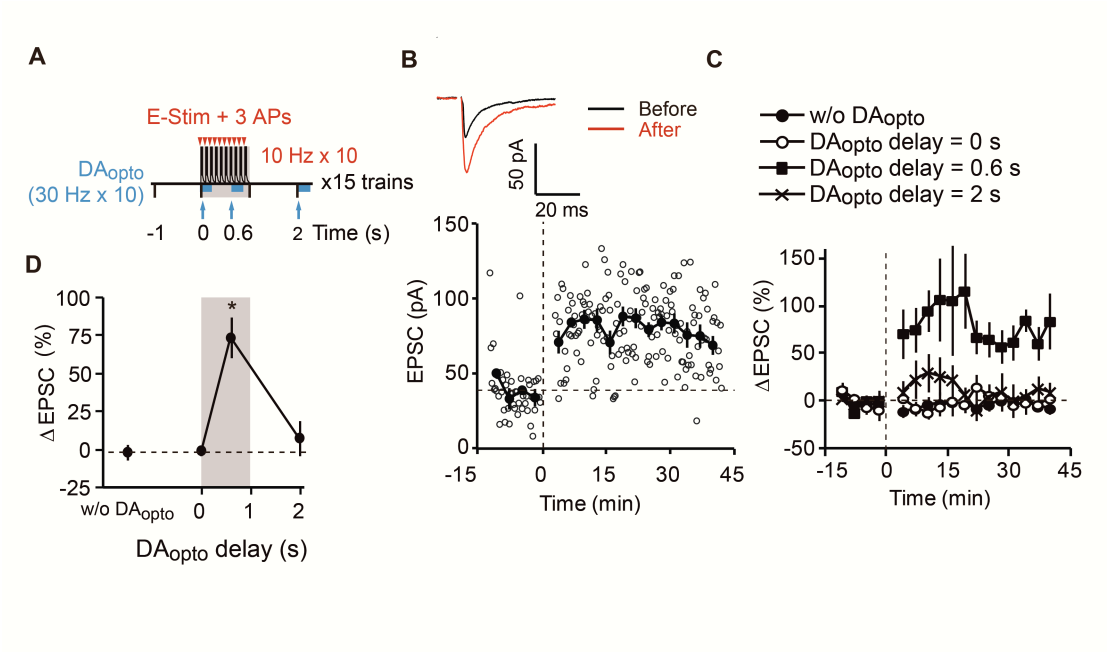

Fig. S4. DA_{opto} timing dependence of long-term potentiation of EPSCs (LTP).

(**A**) The STDP protocol with electrical stimulation of presynaptic fibers (eSTDP). The protocol was the same as Fig. 1I, except that glutamate uncaging was replaced with electrical stimulation. DA_{opto} was applied at three different time points from the onset of eSTDP. (**B**) An example of LTP induced by eSTDP + DA_{opto} with a delay of 0.6 s. Open circles represent the amplitudes of EPSCs evoked by test stimuli applied every 15 s, while filled circles the average amplitudes of 12 successive EPSCs. The inset shows the averaged EPSCs before (black) and 28 to 40 min after induction (red) of LTP. (**C**) The averaged time courses of EPSC amplitudes in response to eSTDP in the absence of DA_{opto} (filled circles, 7 cells) or in the presence of DA_{opto} with delays of 0 s (open circles, 5 cells), 0.6 s (squares, 5 cells), and 2 s (crosses, 6 cells). (**D**) The amplitudes of LTP plotted vs. DA_{opto} delay. $P = 0.0086$ with Kruskal–Wallis and $*P = 0.013$ (0.6 s) by Steel test vs. eSTDP without DA_{opto}. Data are presented as mean ± s.e.m.

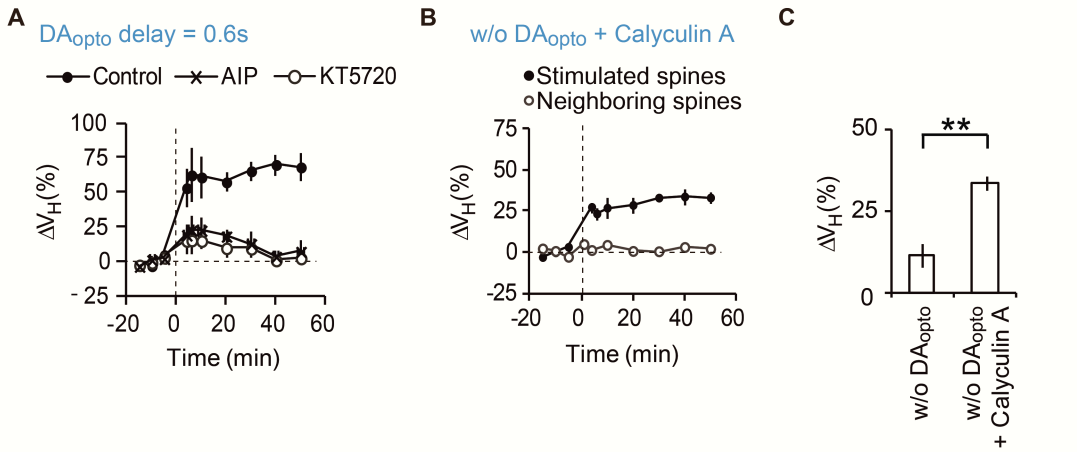

Fig. S5. Pharmacology of spine enlargement.

(**A**) Time courses of spine enlargement induced by STDP + DA_{opto} with a 0.6 s delay in the absence (Control, the same as Fig. 2A) and presence of CaMKII inhibitor (5 μM AIP in the pipette, 20 spines, 5 dendrites) or PKA inhibitor (2 μM KT5720, 20 spines, 5 dendrites). (**B**) Time courses of spine enlargement induced by STDP without DA_{opto} in the presence of PP-1 inhibitor calyculin A (50 nM, 20 spines, 5 dendrites). (**C**) Effect of PP-1 inhibitor on spine volume change induced by STDP stimulation without DA_{opto}. Control value was derived from Fig 1G. Mann Whitney U test. $^{**}P = 0.0031$. Because the control condition of STDP without DA_{opto} was used as controls in other analyses (Fig. 1H, O), we re-analyzed them by including all of the conditions (STDP without DA_{opto} , STDP with dopamine puff, STDP plus DA_{opto} delays of -1 s, 0 s, 0.3 s, 0.6 s, 1 s, 2 s, and 5 s, and STDP without DA_{opto} in the presence of calyculin A) into a single analysis with Kruskal–Wallis test. The results showed significant effect ($P = 4.81\times 10^{-7}$) and post-hoc Steel's test vs. STDP without DA_{opto} revealed significant differences in STDP with dopamine puff ($P = 0.034$, Fig. 1H), STDP plus DA_{opto} delays with 0.6 s ($P = 0.0023$, Fig. 1O) and 1 s ($P = 0.0035$, Fig. 1O), and STDP without DA_{opto} in the presence of calyculin A ($P = 0.034$). Thus all of the significant differences observed in Fig, 1H and O survived multiple comparisons.

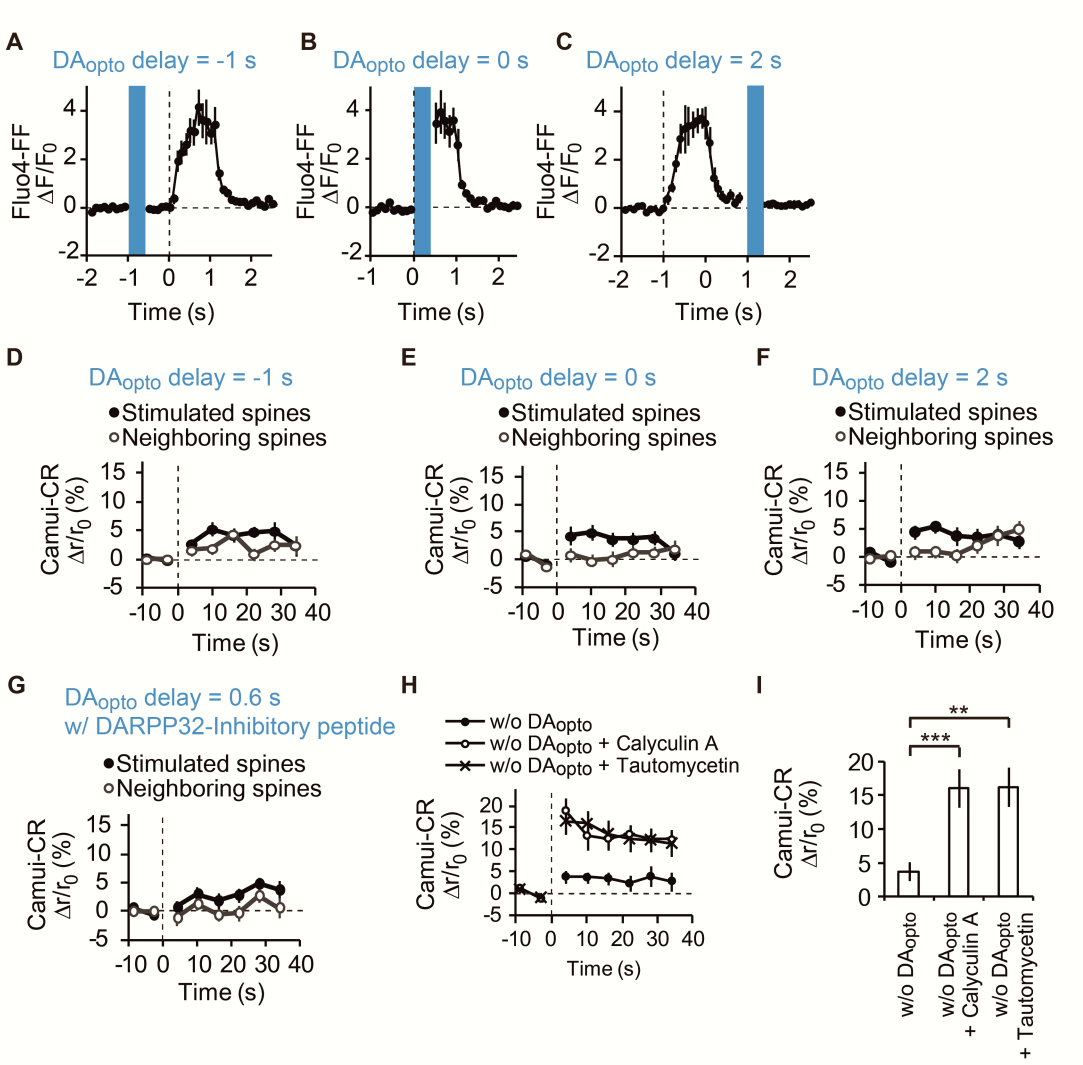

Fig. S6. DA_{opto} modulation of Ca^{2+} and CaMKII signaling.

(**A–C**) Fluo4-FF responses to a single train of STDP + DA_{opto} with delays of –1 s (A, 11 spines, 5 dendrites), 0 s (B, 9 spines, 3 dendrites), and 2 s (C, 11 spines, 5 dendrites). Blue bars indicate the period of blue laser stimulation that disabled the fluorescent measurement. (**D–F**) Camuiα-CR responses to a single train of STDP + DA_{opto} with delays of –1 s (A, 32 spines, 8 dendrites), 0 s (B, 35 spines, 9 dendrites), and 2 s (C, 38 spines, 6 dendrites). (**G**) The effect of DARPP-32-inhibitory peptide on Camuiα-CR responses to a single train of STDP + DA_{opto} with a 0.6-s delay. (**H**) Camuiα-CR responses to a single train of STDP without DA_{opto} in the absence (16 spines, 4 dendrites) and the presence of PP-1 inhibitors, calyculin A (50 nM, 20 spines, 5 dendrites) or tautomycetin (4 nM, 22 spines, 5 dendrites). (**I**) The peak responses of Camuiα-CR ratios in the absence and presence of PP-1 inhibitors. $P = 0.0002$ with Kruskal–Wallis and ***$P = 0.0003$ (calyculin A) and ** $P = 0.0010$ (tautomycetin) by Steel test vs. that in the absence of inhibitor. Data are presented as mean ± s.e.m.

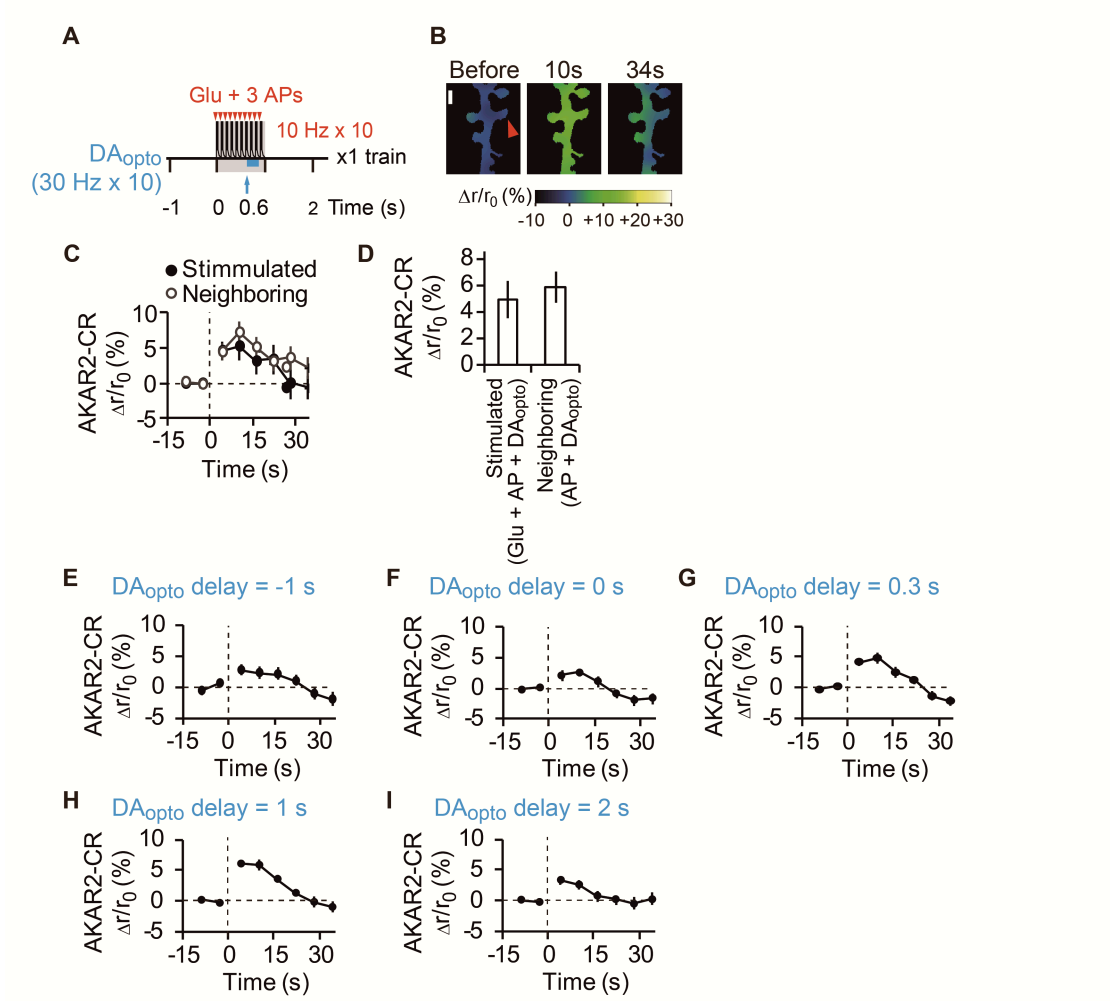

Fig. S7. PKA signaling in response to various DA_{opto} paradigms.

(**A**) One train of STDP + DA_{opto} with a 0.6-s delay to measure PKA activation. (**B**) Images of FRET ratios of AKAR2-CR. A red arrowhead denotes the spine stimulated by caged glutamate. Scale bar, 1 μm. (**C**) The time courses of the ratios in stimulated and neighboring spines (36 spines, 21 dendrites). (**D**) Effects of glutamate uncaging on the AKAR2-CR signals. Both stimulated and neighboring spines showed significant increases in the AKAR2-CR signals compared with baseline. $P = 0.011$ (stimulated) and 1.6×10^{-6} (neighboring) with Mann-Whitney U test. There was no significant difference between them. $P = 0.73$ with Mann-Whitney U test. (**E–I**) Time courses of AKAR2-CR response to APs + DA_{opto} with delays of –1 s (E, 103 spines, 15 dendrites), 0 s (F, 116 spines, 18 dendrites), 0.3 s (G, 85 spines, 12 dendrites), 1 s (H, 81 spines, 11 dendrites), and 2 s (I, 104 spines, 16 dendrites).

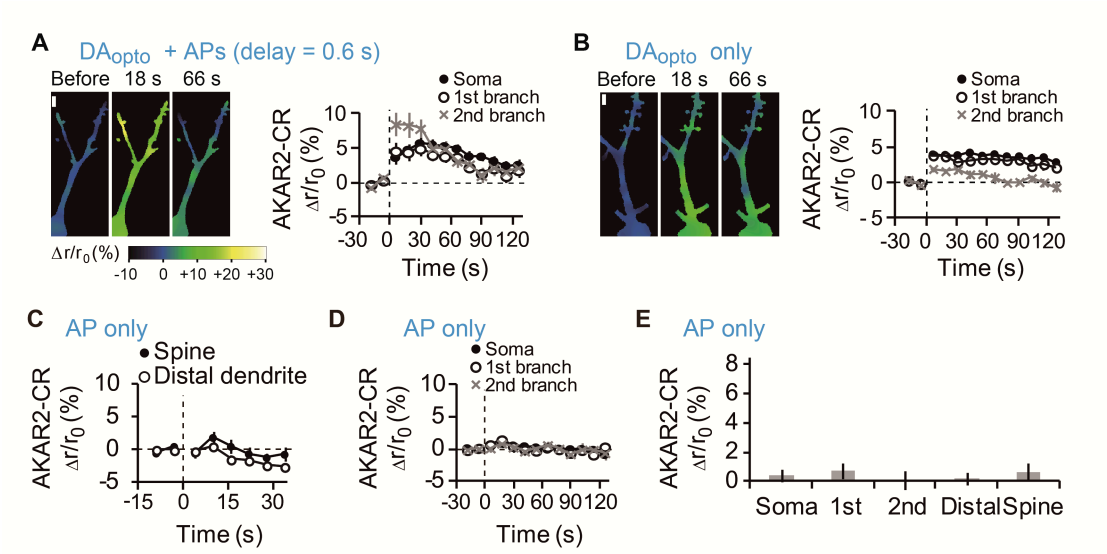

Fig. S8. Subcellular difference in PKA signaling in response to DA_{opto}.

(**A, B**) Time-course of AKAR2-CR responses at the soma and first and second dendrite branches stimulated by APs + DA_{opto} with a 0.6-s delay (A, 11 soma/dendrites) or DA_{opto} only (B, 25 soma/dendrites). DA_{opto} only did not induce significant activation in distal dendrites compared with baseline ($P = 0.12$, 26 dendrites, Mann-Whitney U test). There was a significant effect of subcellular region on AKAR2-CR responses to DA_{opto} only ($P = 4.1 \times 10^{-6}$, Kruskal–Wallis test), and the soma and first branch showed significantly greater responses compared with distal dendrites. $P = 0.0002$ (soma) and 0.0003 (first) with Steel's test. Scale bar, 2 μm. (**C, D**) AP-induced AKAR2-CR responses at the spine and distal dendrites (C, 100 spines, 16 dendrites) and in the soma and first and second dendrite branches (D, 14 soma/dendrites). None of them showed significant increases in the AKAR2-CR signals compared with baseline. $P = 0.49$ (soma), 0.49 (first), 0.17 (second), 1.0 (distal), and 0.053 (spine) with Mann-Whitney U test (not corrected for multiple comparisons). Data are presented as mean ± s.e.m. (**E**) Averaged increases in AKAR2-CR signals in the conditions shown in (C, D).

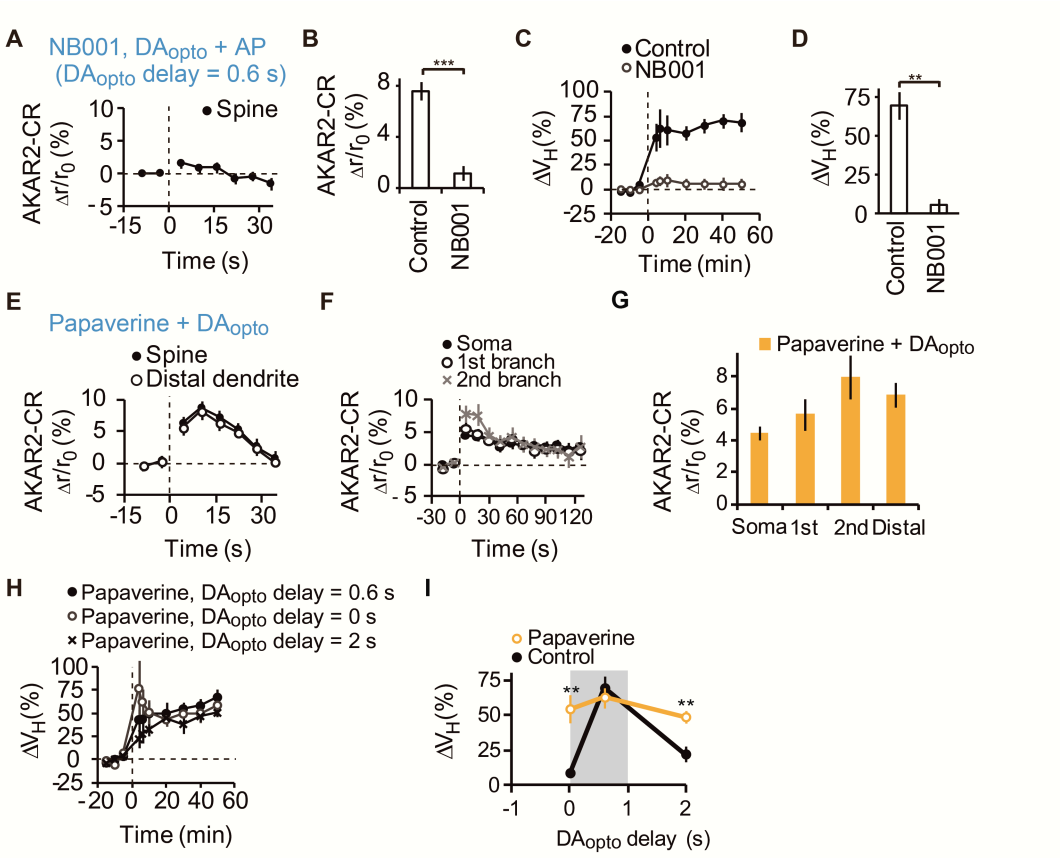

Fig. S9. Dependence of PKA activation on AC1 and PDE10A.

(**A**) Time courses of AKAR2-CR activation by AP + DA_{opto} with a 0.6-s delay in the presence of NB001 (50 μM). (**B**) The peak FRET signals of AKAR2-CR in the absence (153 spines, 25 dendrites, the same data as Fig. 4a) and presence of NB001 (50 μM, 151 spines, 22 dendrites). ***$P = 4.3 \times 10^{-7}$ with Mann-Whitney U test. (**C**)Time courses of spine enlargement induced by STDP + DA_{opto} in the absence (24 spines, 7 dendrites, the same data as Fig. 2a, Control) and presence of NB001 (23 spines, 6 dendrites). (**D**) The enlargement was potently blocked by NB001. ** $P = 0.0027$ with Mann-Whitney U test. (**E**, **F**) The time courses of DA_{opto}-induced AKAR2-CR FRET signals in the presence of papaverine in spines and distal dendrites (E, 143 spines, 22 dendrites), and the soma and first and second dendrite branches (F, 9 soma/dendrites). (**G**) AKAR2 responses to DA_{opto} in the presence of the PDE10A inhibitor papaverine. They were not dependent on subcellular regions ($P = 0.09$, Kruskal–Wallis test). (**H**) The traces of spine enlargement induced by STDP and DA_{opto} with delays of 0.6 s (23 spines, 6 dendrites), 0 s (24 spines, 6 dendrites), or 2 s (24 spines, 6 dendrites) in the presence of papaverine. (**I**) Papaverine effects on DA_{opto} timing on spine enlargement. **$P = 0.0011$ (0 s) and 0.0066 (2 s), Mann-Whitney U test vs. the control values derived from Fig. 1O. Data are presented as mean ± s.e.m.

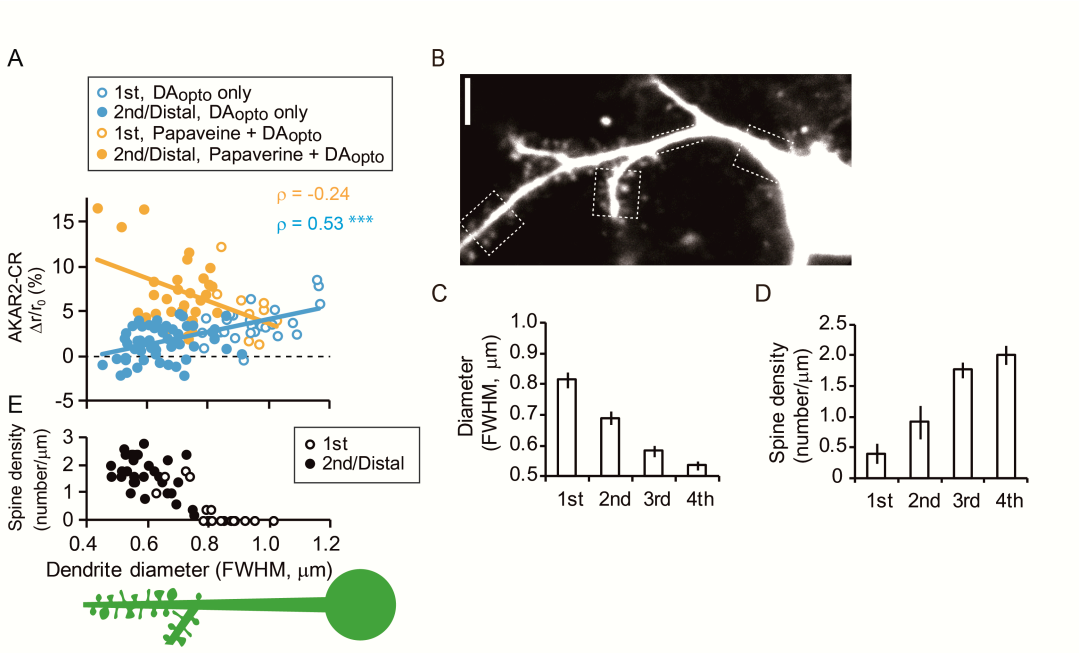

Fig. S10. Dendritic diameters and spine densities in MSNs.

(**A**) Dependence of DA_{opto}-evoked AKAR2-CR signals on dendritic diameters quantified by full-width-at-half-maximal (FWHM) diameters. The Spearman's correlation coefficients were $\rho = 0.53$ (***$P = 7.6 \times 10^{-7}$, 76 dendrites) in control, and $\rho = -0.24$ ($P = 0.13$, 40 dendrites) in the presence of papaverine. (**B**) A representative image of an MSN that was whole-cell perfused with Alexa 488. Scale bar, 5 μm. The dotted boxes indicate the first, second, third, and fourth branches of dendrites. (**C**, **D**) Average diameters (C) and spine density (D) of dendrites for each branch (51 dendritic branches, 6 cells). (**E**) The spine densities along MSN dendrites. Spines were only present in dendrites thinner than 0.8 μm, as illustrated in the diagram.

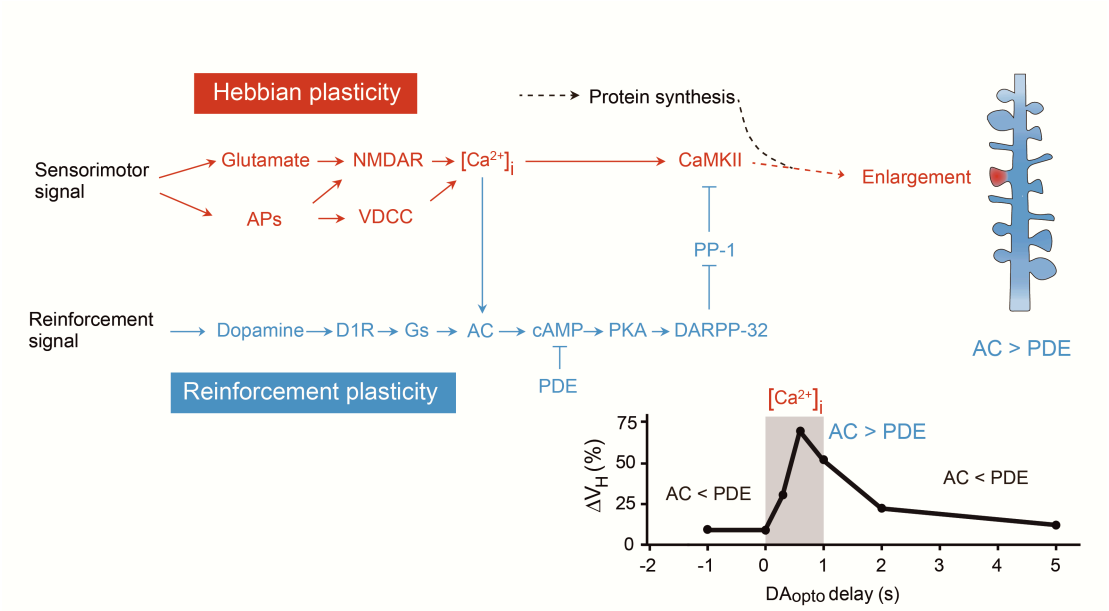

Fig. S11. A signaling scheme for Hebbian and reinforcement plasticity in synaptic spines.

Signaling cascades for reinforcement and Hebbian plasticity of dendritic spines in MSNs. Concurrent activation of presynaptic inputs (glutamate) and postsynaptic APs results in Ca^{2+} influx through NMDARs that stimulate CaMKII. This Hebbian mechanism is not sufficient to fully activate CaMKII; rather, it requires reinforcement by PKA-DARPP-32-PP1 signaling. PKA activation requires APs and subsequent dopamine to overcome the high phosphodiesterase activity in thin distal dendrites. Thus, the balance of activity between phosphodiesterase and Ca^{2+}-dependent adenylate cyclase shapes the temporal window for dopamine's effects on PKA activation and spine enlargement. Because these molecules are expressed in synaptic spines in various brain regions, analogous mechanisms may occur throughout the brain, particularly in those neurons with spines and thin dendrites (Fig. 4D, E).

References and Notes

1. E. L. Thorndike, *Animal Intelligence* (Macmillan, New York, 1911).

2. I. P. Pavlov, *Conditioned Reflexes; An Investigation of the Physiological Activity of the Cerebral Cortex* (Oxford Univ. Press, Humphrey Milford, London, 1927).

3. M. F. Roitman, R. A. Wheeler, R. M. Carelli, Nucleus accumbens neurons are innately tuned for rewarding and aversive taste stimuli, encode their predictors, and are linked to motor output. *Neuron* **45**, 587–597 (2005). Medline doi:10.1016/j.neuron.2004.12.055

4. Y. Dan, M. M. Poo, Spike timing-dependent plasticity: From synapse to perception. *Physiol. Rev.* **86**, 1033–1048 (2006). Medline doi:10.1152/physrev.00030.2005

5. J. Black, J. D. Belluzzi, L. Stein, Reinforcement delay of one second severely impairs acquisition of brain self-stimulation. *Brain Res.* **359**, 113–119 (1985). Medline doi:10.1016/0006-8993(85)91418-0

6. W. Schultz, Predictive reward signal of dopamine neurons. *J. Neurophysiol.* **80**, 1–27 (1998). Medline

7. S. L. Smith-Roe, A. E. Kelley, Coincident activation of NMDA and dopamine D1 receptors within the nucleus accumbens core is required for appetitive instrumental learning. *J. Neurosci.* **20**, 7737–7742 (2000). Medline

8. T. Nakano, J. Yoshimoto, K. Doya, A model-based prediction of the calcium responses in the striatal synaptic spines depending on the timing of cortical and dopaminergic inputs and post-synaptic spikes. *Front. Comput. Neurosci.* **7**, 119 (2013). Medline doi:10.3389/fncom.2013.00119

9. M. Matsuzaki, G. C. Ellis-Davies, T. Nemoto, Y. Miyashita, M. Iino, H. Kasai, Dendritic spine geometry is critical for AMPA receptor expression in hippocampal CA1 pyramidal neurons. *Nat. Neurosci.* **4**, 1086–1092 (2001). Medline doi:10.1038/nn736

10. M. Matsuzaki, N. Honkura, G. C. R. Ellis-Davies, H. Kasai, Structural basis of long-term potentiation in single dendritic spines. *Nature* **429**, 761–766 (2004). Medline doi:10.1038/nature02617

11. J. Tanaka, Y. Horiike, M. Matsuzaki, T. Miyazaki, G. C. Ellis-Davies, H. Kasai, Protein synthesis and neurotrophin-dependent structural plasticity of single dendritic spines. *Science* **319**, 1683–1687 (2008). Medline doi:10.1126/science.1152864

12. C. D. Harvey, R. Yasuda, H. Zhong, K. Svoboda, The spread of Ras activity triggered by activation of a single dendritic spine. *Science* **321**, 136–140 (2008). Medline doi:10.1126/science.1159675

13. C. R. Gerfen, T. M. Engber, L. C. Mahan, Z. Susel, T. N. Chase, F. J. Monsma Jr., D. R. Sibley, D1 and D2 dopamine receptor-regulated gene expression of striatonigral and striatopallidal neurons. *Science* **250**, 1429–1432 (1990). Medline doi:10.1126/science.2147780

14. W. Shen, M. Flajolet, P. Greengard, D. J. Surmeier, Dichotomous dopaminergic control of striatal synaptic plasticity. *Science* **321**, 848–851 (2008). Medline doi:10.1126/science.1160575

15. J. N. J. Reynolds, B. I. Hyland, J. R. Wickens, A cellular mechanism of reward-related learning. *Nature* **413**, 67–70 (2001). Medline doi:10.1038/35092560

16. R. A. Rescorla, Behavioral studies of Pavlovian conditioning. *Annu. Rev. Neurosci.* **11**, 329–352 (1988). Medline doi:10.1146/annurev.ne.11.030188.001553

17. Y. G. Kwon, H. B. Huang, F. Desdouits, J. A. Girault, P. Greengard, A. C. Nairn, Characterization of the interaction between DARPP-32 and protein phosphatase 1 (PP-1): DARPP-32 peptides antagonize the interaction of PP-1 with binding proteins. *Proc. Natl. Acad. Sci. U.S.A.* **94**, 3536–3541 (1997). Medline doi:10.1073/pnas.94.8.3536

18. R. D. Blitzer, J. H. Connor, G. P. Brown, T. Wong, S. Shenolikar, R. Iyengar, E. M. Landau, Gating of CaMKII by cAMP-regulated protein phosphatase activity during LTP. *Science* **280**, 1940–1943 (1998). Medline doi:10.1126/science.280.5371.1940

19. C. Cepeda, M. S. Levine, Where do you think you are going? The NMDA-D1 receptor trap. *Sci. STKE* **2006**, pe20 (2006). Medline

20. K. Takao, K. Okamoto, T. Nakagawa, R. L. Neve, T. Nagai, A. Miyawaki, T. Hashikawa, S. Kobayashi, Y. Hayashi, Visualization of synaptic Ca^{2+}/calmodulin-dependent protein kinase II activity in living neurons. *J. Neurosci.* **25**, 3107–3112 (2005). Medline doi:10.1523/JNEUROSCI.0085-05.2005

21. S. J. R. Lee, Y. Escobedo-Lozoya, E. M. Szatmari, R. Yasuda, Activation of CaMKII in single dendritic spines during long-term potentiation. *Nature* **458**, 299–304 (2009). Medline doi:10.1038/nature07842

22. A. J. Lam, F. St-Pierre, Y. Gong, J. D. Marshall, P. J. Cranfill, M. A. Baird, M. R. McKeown, J. Wiedenmann, M. W. Davidson, M. J. Schnitzer, R. Y. Tsien, M. Z. Lin, Improving FRET dynamic range with bright green and red fluorescent proteins. *Nat. Methods* **9**, 1005–1012 (2012). Medline doi:10.1038/nmeth.2171

23. G. D. Ferguson, D. R. Storm, Why calcium-stimulated adenylyl cyclases? *Physiology (Bethesda)* **19**, 271–276 (2004). Medline doi:10.1152/physiol.00010.2004

24. L. R. V. Castro, M. Brito, E. Guiot, M. Polito, C. W. Korn, D. Hervé, J. A. Girault, D. Paupardin-Tritsch, P. Vincent, Striatal neurones have a specific ability to respond to phasic dopamine release. *J. Physiol.* **591**, 3197–3214 (2013). Medline

25. A. Nishi, M. Kuroiwa, D. B. Miller, J. P. O'Callaghan, H. S. Bateup, T. Shuto, N. Sotogaku, T. Fukuda, N. Heintz, P. Greengard, G. L. Snyder, Distinct roles of PDE4 and PDE10A in the regulation of cAMP/PKA signaling in the striatum. *J. Neurosci.* **28**, 10460–10471 (2008). Medline doi:10.1523/JNEUROSCI.2518-08.2008

26. E. I. Charych, L. X. Jiang, F. Lo, K. Sullivan, N. J. Brandon, Interplay of palmitoylation and phosphorylation in the trafficking and localization of phosphodiesterase 10A: Implications for the treatment of schizophrenia. *J. Neurosci.* **30**, 9027–9037 (2010). Medline doi:10.1523/JNEUROSCI.1635-10.2010

27. C. J. Wilson, P. M. Groves, Fine structure and synaptic connections of the common spiny neuron of the rat neostriatum: A study employing intracellular inject of horseradish peroxidase. *J. Comp. Neurol.* **194**, 599–615 (1980). Medline doi:10.1002/cne.901940308

28. R. D. Hawkins, T. W. Abrams, T. J. Carew, E. R. Kandel, A cellular mechanism of classical conditioning in Aplysia: Activity-dependent amplification of presynaptic facilitation. *Science* **219**, 400–405 (1983). Medline doi:10.1126/science.6294833

29. Y. Yovell, T. W. Abrams, Temporal asymmetry in activation of Aplysia adenylyl cyclase by calcium and transmitter may explain temporal requirements of conditioning. *Proc. Natl. Acad. Sci. U.S.A.* **89**, 6526–6530 (1992). Medline doi:10.1073/pnas.89.14.6526

30. R. S. Sutton, A. G. Barto, *Reinforcemnet Learning* (MIT Press, Cambridge, MA, 1998).

31. T. Hikida, K. Kimura, N. Wada, K. Funabiki, S. Nakanishi, Distinct roles of synaptic transmission in direct and indirect striatal pathways to reward and aversive behavior. *Neuron* **66**, 896–907 (2010). Medline doi:10.1016/j.neuron.2010.05.011

32. J. C. Grieger, V. W. Choi, R. J. Samulski, Production and characterization of adeno-associated viral vectors. *Nat. Protoc.* **1**, 1412–1428 (2006). Medline doi:10.1038/nprot.2006.207

33. H. Wang, H. Xu, L. J. Wu, S. S. Kim, T. Chen, K. Koga, G. Descalzi, B. Gong, K. I. Vadakkan, X. Zhang, B. K. Kaang, M. Zhuo, Identification of an adenylyl cyclase inhibitor for treating neuropathic and inflammatory pain. *Sci. Transl. Med.* **3**, 65ra3 (2011). Medline doi:10.1126/scitranslmed.3001269

34. G. Corder, S. Doolen, R. R. Donahue, M. K. Winter, B. L. Jutras, Y. He, X. Hu, J. S. Wieskopf, J. S. Mogil, D. R. Storm, Z. J. Wang, K. E. McCarson, B. K. Taylor, Constitutive μ-opioid receptor activity leads to long-term endogenous analgesia and dependence. *Science* **341**, 1394–1399 (2013). Medline doi:10.1126/science.1239403

35. G. C. Ellis-Davies, M. Matsuzaki, M. Paukert, H. Kasai, D. E. Bergles, 4-Carboxymethoxy-5,7-dinitroindolinyl-Glu: An improved caged glutamate for expeditious ultraviolet and two-photon photolysis in brain slices. *J. Neurosci.* **27**, 6601–6604 (2007). Medline doi:10.1523/JNEUROSCI.1519-07.2007

36. Y. Matsuda, A. Marzo, S. Otani, The presence of background dopamine signal converts long-term synaptic depression to potentiation in rat prefrontal cortex. *J. Neurosci.* **26**, 4803–4810 (2006). Medline doi:10.1523/JNEUROSCI.5312-05.2006

37. F. Tecuapetla, J. C. Patel, H. Xenias, D. English, I. Tadros, F. Shah, J. Berlin, K. Deisseroth, M. E. Rice, J. M. Tepper, T. Koos, Glutamatergic signaling by mesolimbic dopamine neurons in the nucleus accumbens. *J. Neurosci.* **30**, 7105–7110 (2010). Medline doi:10.1523/JNEUROSCI.0265-10.2010

38. N. X. Tritsch, J. B. Ding, B. L. Sabatini, Dopaminergic neurons inhibit striatal output through non-canonical release of GABA. *Nature* **490**, 262–266 (2012). Medline doi:10.1038/nature11466

39. N. L. Xu, M. T. Harnett, S. R. Williams, D. Huber, D. H. O'Connor, K. Svoboda, J. C. Magee, Nonlinear dendritic integration of sensory and motor input during an active sensing task. *Nature* **492**, 247–251 (2012). Medline doi:10.1038/nature11601